Brittlestar-Inspired Microlens Arrays Made of Calcite Single Crystals

*Xiaozhou Ye, Fei Zhang, Yurong Ma, and Limin Qi**

Nature produces a vast variety of intricate biominerals consisting of simple constituents yet exhibiting remarkable multifunctional properties.[1,2] In particular, light-sensitive brittlestars form highly sophisticated microlens arrays made of calcite single crystals, which show exceptional optical performance while offering mechanical protection.[3] It has long been an attractive goal to produce crystalline materials with structures and properties resembling those of natural biominerals.[4–6] Although considerable progress has been made in the bioinspired fabrication of patterned calcite single crystals[7,8] and microlens arrays made of amorphous[9,10a] and polycrystalline[10b] materials, it remains a challenge to produce single crystal microlens arrays mimicking brittlestar's microlenses. Here we show that microlens arrays made of calcite single crystals with tunable orientations can be readily fabricated by template-assisted epitaxial growth under ambient conditions, which sheds new light on biological calcification processes. The single crystal microlens arrays demonstrate orientation-dependent imaging performance and exhibit remarkable polarization-dependent optical properties, showing their potential applications in integral imaging[11,12] and micro- and nano-optics.[13,14]

Microlens arrays (MLAs) are two-dimensional (2D) arrays of miniaturized lenses with diameters ranging from several micrometers to nearly a millimeter, which have a broad range of applications such as micro-optical devices for light collimating, spreading, and coupling,[15] efficiency enhancement in light-emitting devices,[16,17] three-dimensional (3D) imaging,[11] single molecule bioimaging,[18] and artificial compound eyes.[19] Till now, the controllable fabrication of convex and concave MLAs comprising varied materials including glasses,[15] amorphous and polycrystalline minerals,[10] polymers,[20,21] protein hydrogels,[22] and liquid crystals[23] has been achieved using various methods. However, it remains a challenging task to fabricate microlenses made of single crystals although a microlens combined with a birefringent crystal can exert control over both the temporal and spatial distribution of light and show interesting properties such as 3D focus manipulation[24] and polarization-dependent focusing.[14] As a typical linearly birefringent crystal, calcite has been widely used for control and characterization of the polarization states of light,[14,24,25] but the controllable fabrication of MLAs built from calcite single crystals has not been realized so far. Amazingly, the natural skeletons of light-sensitive brittlestars adopt an elaborate structure of microlens arrays made of calcite single crystals oriented along the optical *c* axis, exhibiting remarkable optical performance originating from the optimized shape and crystal orientation.[3] Since their discovery, the nearly perfect microlens arrays in brittlestars have been used as an inspirational system for the design and synthesis of novel optical elements.[26] Notably, the bioinspired fabrication of micropatterned[7] and nanopatterned[8e,g] calcite single crystals was successfully achieved through template-directed deposition and crystallization of amorphous calcium carbonate.

As a strategy borrowed from the biomineralization principles existing in certain biological systems, crystallization from an amorphous precursor has been considered as an attractive route toward templated single crystals.[4,7] However, the impurity release and volume shrinkage accompanying crystallization from prefilled amorphous phase are unfavorable for a faithful replication of large single crystals. On other hand, template-assisted growth of calcite single crystals via ion-by-ion approaches has turned out to be effective for the synthesis of calcite single crystals with complex morphologies.[8a-d] For example, micrometer-sized single crystals of calcite with patterned surfaces comprising concave lenses were produced by crystallization on colloidal monolayers[8c] or using colloidal templates.[8f] However, it remains a challenge to achieve large-scale, optically functional, calcite single crystals with highly ordered patterns and tunable crystallographic orientations. Herein, we developed a novel crystallization strategy based on templating against monolayer colloidal crystals (MCCs)[27] combined with the epitaxial growth on large-area calcite single crystal substrates. This template-assisted epitaxial growth strategy allows for facile fabrication of optically functional, concave microlens arrays consisting of calcite single crystals with controlled crystallographic orientations, which are reminiscent of the brittlestar's convex microlens arrays.

For the fabrication of concave MLAs made of calcite single crystals, a monolayer colloidal crystal of polystyrene (PS) microspheres (~6 μm in diameter) was first assembled on the top surface of a calcite plate (~1 mm in thickness

X. Ye, F. Zhang, Prof. Y. Ma, Prof. L. Qi
Beijing National Laboratory for Molecular Sciences (BNLMS)
State Key Laboratory for Structural Chemistry of Unstable and Stable Species
College of Chemistry
Peking University
Beijing 100871, China
E-mail: liminqi@pku.edu.cn

DOI: 10.1002/smll.201402765

www.MaterialsViews.com

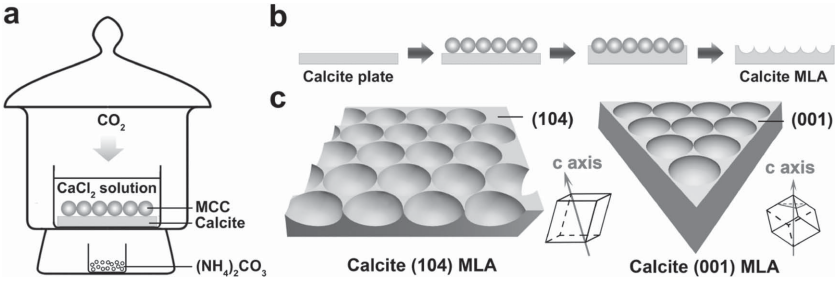

Figure 1. Schematic illustration for the fabrication of single crystal calcite microlens arrays (MLAs). a) Experimental setup for the formation of calcite MLA. b) Formation of calcite MLA through MCC-assisted, epitaxial growth on calcite plate. c) Structure and crystal orientation of calcite (104) and (001) MLAs. The optical axis of rhombohedral calcite crystal is along the c axis indicated by the arrows. The calcite (001) plane can be exposed by grinding away one corner of a calcite rhombohedron enclosed by {104} planes.

and typically larger than 10 mm^2 in size). The MCC-covered calcite plate was then immersed in an aqueous $CaCl_2$ solution, which was placed in a closed desiccator for the epitaxial growth of calcite induced by CO_2 diffusion (**Figure 1**a). After an appropriate growth time, the lower PS hemispheres were completely embedded in calcite crystals and then the PS spheres were removed, resulting in the formation of a concave calcite MLA (Figure 1b). Single crystal calcite plates with the top surfaces of the (104) and (001) planes were employed for the epitaxial growth of single crystal calcite (104) and (001) MLAs, respectively (Figure 1c). The optical *c* axis was perpendicular to the array plane for the calcite (001) MLA whereas it was inclined for the calcite (104) MLA.

The integration of an MCC of PS spheres on a calcite plate was achieved by self-assembly at the gas-liquid interface followed by transfer onto the substrate using the previously reported method.[28] **Figure 2**a shows a typical scanning electron microscopy (SEM) image of a hexagonal-close-packed (hcp) MCC formed on a (104)-oriented calcite plate, where the PS spheres attached closely to the top surface of the substrate (Figure 2b). After 2 h of epitaxial growth at room temperature, the PS spheres were partially embedded in the grown calcite crystal, leading to the formation of non-close-packed arrays of spherical cavities with a height less than their radius after MCC removal (Figure 2c). When the growth time was prolonged to 4 h, the lower PS hemispheres were almost completely embedded in the grown calcite crystal (Figure 2d). After MCC removal, regular hcp arrays of hemispherical cavities were obtained (Figure 2e), indicating the formation of a uniform concave MLA. A side-view of the edge of the calcite MLA (Figure 2f) suggests that the hemispherical cavities had a height nearly identical to their radius (~ 3 μm). A high-magnification SEM image (Figure 2g) shows that the inner surface of the hemispherical cavitiy was very smooth, indicating a faithful replication of the MCC template. The X-ray diffraction (XRD) pattern of a single concave MLA (Figure 2h) exhibits only sharp diffraction peaks arising from the (104) and (208) reflections of calcite, confirming the formation of an MLA made of a (104)-oriented calcite single crystal, namely, a calcite (104) MLA.

Similarly, a calcite (001) MLA with the optical *c* axis perpendicular to the 2D array plane can be fabricated using a (001)-oriented calcite plate as the substrate for MCC-assisted epitaxial growth. After 3 h of epitaxial growth at room temperature, the MCC covering the calcite (001) plate was partially embedded in the grown crystal with a relatively coarse surface (**Figure 3**a,b). After MCC removal, unconnected cavities with a height less than their radius were obtained (Figure 3c). Interestingly, numerous tiny triangular pyramids with exposed {104} facets that have much lower surface energy[29] appeared in the areas between cavities, confirming an epitaxial growth on the calcite (001) plane. When the growth time was prolonged to 6 h, the lower hemispheres were almost completely embedded in the grown calcite crystal (Figure 3d). Then, a uniform concave MLA consisting of regular hcp arrays of hemispherical cavities was obtained after MCC removal (Figure 3e). The top surface of the concave MLA grown on the calcite (001) plate was rather coarse (Figure 3f), but the inner surface of the cavities was very smooth (Figure 3g). This result suggests that a faithful replication of the MCC template was also achieved although triangular pyramids tended to form in the triangular areas between the unconnected cavities. The XRD pattern of a single MLA (Figure 3h) exhibits only sharp diffraction peaks arising from the (006) and (0 0 12) reflections of calcite, confirming the formation of an MLA made of a (001)-oriented calcite single crystal. The artificial concave calcite (001) MLA is reminiscent of the natural convex calcite (001) MLAs formed by brittlestars.[3]

The single-crystalline nature of the produced calcite MLAs was further demonstrated by the overgrowth experiments (Figure S1, Supporting Information). The calcite (104) MLA after overgrowth exhibited uni-oriented

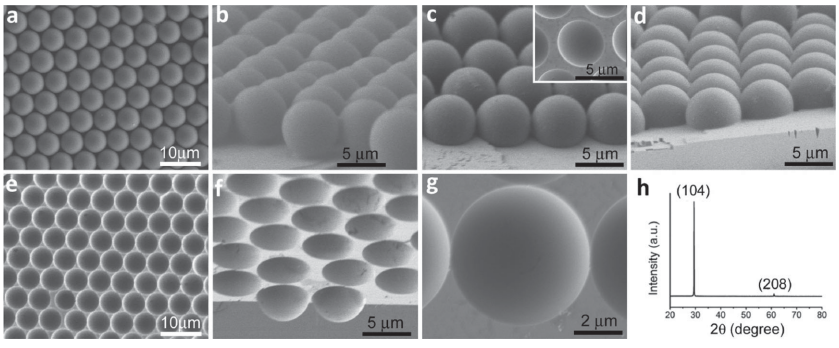

Figure 2. Formation of single crystal calcite (104) MLA. a,b) Top-view and side-view SEM images of MCC-covered, (104)-oriented calcite plate, respectively. c) SEM image of MCC-embedded calcite plate after expitaxial growth for 2 h. Inset shows the resultant calcite plate with spherical cavities after MCC removal. SEM images of d) MCC-embedded calcite plate after expitaxial growth for 4 h, and e-g) the resultant calcite (104) MLA after MCC removal. h) XRD pattern of calcite (104) MLA, showing the exclusive (104) orientation.

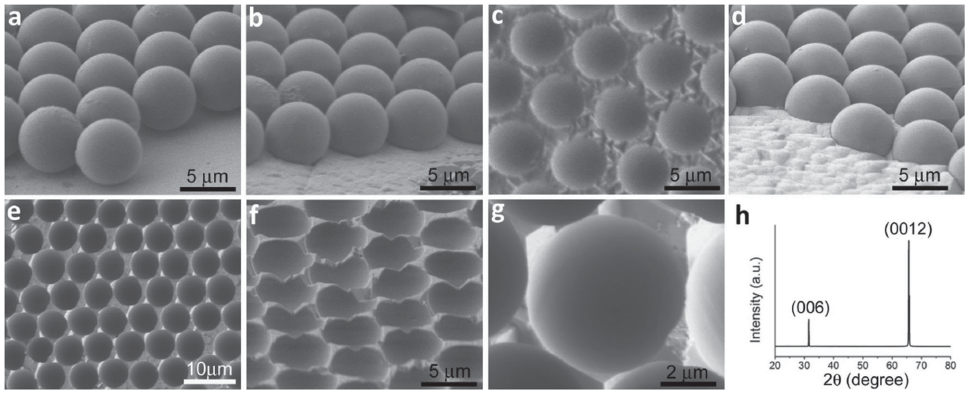

Figure 3. Formation of single crystal calcite (001) MLA. a) SEM image of MCC-covered, (001)-oriented calcite plate. b,c) SEM images of MCC-embedded calcite plate after expitaxial growth for 3 h and the resultant calcite plate with spherical cavities after MCC removal, respectively. SEM images of d) MCC-embedded calcite plate after expitaxial growth for 6 h, and e-g) the resultant calcite (001) MLA after MCC removal. h) XRD pattern of calcite (001) MLA, showing the exclusive (001) orientation.

rhombohedrons with exposed (104) facets, indicating an epitaxial relationship to the calcite (104) substrate. In contrast, the calcite (001) MLA after overgrowth exhibited uni-oriented triangular pyramids dominated by the {104} facets, in good agreement with an epitaxial growth the calcite (001) substrate. Therefore, the MCC-assisted epitaxial growth provided a mild and feasible route toward fabrication of concave MLAs made of calcite single crystals with tunable orientations. In addition, it is worth mentioning that the cavity diameter of single crystal calcite MLAs can be readily adjusted by using the MCC templates made of PS spheres with different diameters (Figure S2, Supporting Information). It may be noted that similar control over the spacing between cavities of concave lens arrays can be achieved for silica deposition around PS MCCs by controlling the PS sphere size and the self-assembly parameters.[30] Therefore, the template-assisted epitaxial growth provides a feasible strategy for simultaneous control over the morphology and orientation of the templated crystals, which has rarely been realized previously.[7] Moreover, the templated calcite single crystals with arrayed hemispherical cavities may find potential applications as unique concave microlens arrays.

Owing to the linearly birefringent characteristics of calcite crystals, the produced MLAs made of calcite single crystals exhibited pronounced orientation-dependent imaging performance (**Figure 4**). Optical microscopy (OM) transmission images of the calcite (104) and (001) MLAs show the regular alignment of uniform microlenses ~ 6 μm in diameter (Figure 4b,c). When the concave MLAs were illuminated by a white light through a projection mask containing a single letter "A" ~1 cm in size (Figure 4a), an array of virtual images of "A" was clearly captured by an objective lens for both the (104) and (001) MLAs (Figure 4d,e). The projected images of "A" are uniform in size and shape, which indicates the rather uniform focal lengths and fine imaging property of the calcite microlenses. However, the difference in the imaging performance for the calcite MLAs with different orientations became evident if a much smaller object was imaged. For example, when a human hair ~ 70 μm in diameter was employed as the projection mask (Figure 4f), an array of double images of the hair was obtained for the calcite (104) MLA (Figure 4g and Figure S3, Supporting Information) whereas an array of clear single images of the hair was captured for the calcite (001) MLA (Figure 4h). It is known that one of the rays passing through a birefringent crystal travels with the same velocity in every direction through the crystal, and is termed the ordinary ray, whereas the other ray travels with a velocity that is

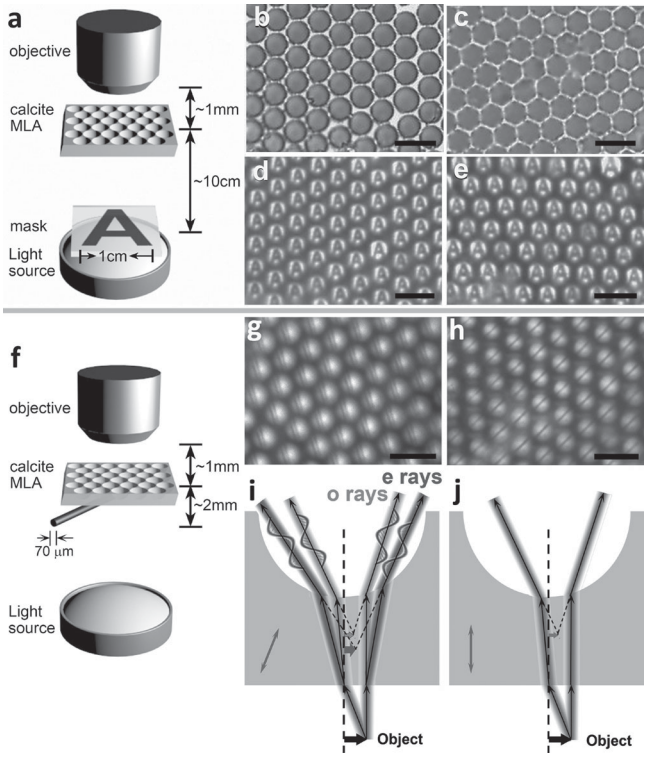

Figure 4. Optical imaging performance of single crystal calcite MLAs. a) Schematic setup of the optical system for imaging a centimeter-sized letter "A". b,c) OM images of calcite (104) and (001) MLAs, respectively. d,e) OM images of "A" arrays projected by calcite (104) and (001) MLAs, respectively. f) Schematic setup of the optical system for imaging a human hair. g,h) OM images of hair arrays projected by calcite (104) and (001) MLAs, respectively. i,j) Schematic illustration of optical paths of light propagated through calcite (104) and (001) MLAs, respectively. The double arrows represent the projected directions of the optical axes of calcite MLAs. Scale bars are 10 μm.

dependent upon the propagation direction within the crystal, and is termed the extraordinary ray. Since calcite is a uniaxial birefringent crystal, and the light propagating through calcite along any directions other than the optical *c* axis splits into ordinary rays (o rays) and extraordinary rays (e rays), which have different refraction indices and polarization states. Therefore, double virtual images were projected by a concave calcite (104) microlens due to different focus lengths for the o and e rays (Figure 4i) whereas a single virtual image was projected by a concave calcite (001) microlens where the incident light is nearly along the non-birefringent optical *c* axis (Figure 4j). It may be noted that the concave MLA made of non-birefringent epoxy also projected a single virtual image (Figure S4a-d, Supporting Information), confirming the non-birefringent characteristic of the calcite (001) microlens. This result shows the first experimental demonstration for the superior optical imaging performance of the (001)-oriented calcite MLAs compared with the calcite MLAs with other orientations, coinciding with the natural selection of the birefringence-free, (001)-oriented calcite MLAs in brittlestars. Despite the undesirable properties for normal optical imaging, the calcite (104) MLAs showing considerable birefringence may exhibit advantageous features for certain applications including advanced nano-optics[14] and integral imaging,[31] where control and utilization of the polarization state of projected light are important.

The polarization-dependent optical properties of the single crystal calcite MLAs with different orientations were evaluated by conoscopic observation using polarized optical microscopy (POM), as shown in **Figure 5**a. The POM images of the birefringence-free calcite (001) MLA suggest that each microlens showed a Maltese cross-like pattern[23b] irrespective to the rotation angle of the MLA in the array plane (Figure 5b). When a linearly polarized light enters a uniaxial crystal, it splits into an ordinary ray and an extraordinary ray with their polarization directions perpendicular and parallel to the plane defined by the propagation direction and the optical axis, respectively. The polarized cone light can not pass both the calcite (001) microlens and the analyzer in the regions that are approximately parallel or perpendicular to the polarizer direction,

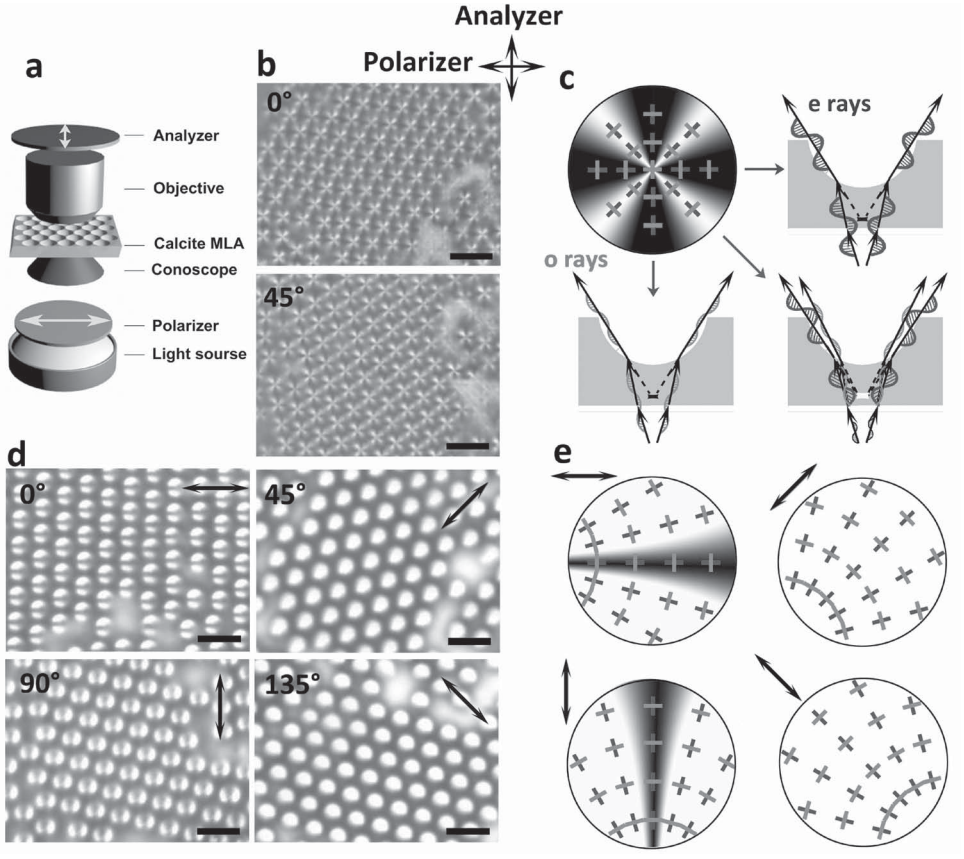

Figure 5. Polarized optical microscopy properties of single crystal calcite MLAs. a) Schematic setup of the optical system for conoscopic observation of calcite MLAs between two crossed polarizers. b) POM images of calcite (001) MLAs with different rotation angles. c) Schematic illustration of the pattern formation of calcite (001) MLAs. Upper left: Simulation of the distribution of transmitted polarized light through calcite (001) microlens. The cross made of deep and light grey lines represents the distribution of the projected direction of polarized rays through calcite (001) MLAs. The deep and light grey lines denote the projected polarization direction of ordinary rays and extraordinary rays, respectively. The sectional views of light paths of three special planes in the upper left picture are illustrated in the pictures of upper right, down left, and down right, respectively. d) POM images of calcite (104) MLAs with different rotation angles. e) Schematic illustration of the pattern formation of calcite (104) MLAs in different angles between the projected direction of the optical axis and the polarizer direction. The deep and light grey lines represent the projected polarization directions of ordinary rays and extraordinary rays, respectively. The double arrows represent the projected directions of the optical axis of calcite (104) MLAs. Scale bars are 10 μm.

resulting in the white cross pattern within each microlens (Figure 5c). In contrast, the POM images of the birefringent calcite (104) MLA show that each microlens exhibited a pattern dependent on the rotation angle between the projected direction of the optical axis and the polarizer direction (Figure 5d). A horizontal black stripe and a longitudinal black stripe appeared when the projected direction of the optical axis was parallel and perpendicular to the polarizer direction, respectively, indicating a unique polarization-dependent property. This result can be rationalized by analyzing the polarization directions of the lights in calcite (104) MLA with different rotation angles (Figure 5e). It may be noted that the non-birefringent resin MLA, which exhibited an imaging performance similar to that of the calcite (001) MLA, just showed a completely dark POM image (Figure S4e,f, Supporting Information). Therefore, the unique birefringent MLAs made of calcite single crystals with polarization selectivity may offer a new platform for the investigation of polarization-dependent micro- and nano-optics.

In conclusion, we have demonstrated that novel concave microlens arrays made of calcite single crystals that essentially resemble the exceptional convex microlens arrays produced by brittlestars can be readily fabricated by template-assisted epitaxial growth in solution without additives under ambient conditions. This strategy provides a facile, feasible and flexible approach toward single crystal microlens arrays since the crystallographic orientation and the microlens parameters can be adjusted separately by selecting desirable substrates and templates. While the non-birefringent calcite (001) microlens array showed an excellent imaging performance like brittlestar's microlens arrays, the birefringent calcite (104) microlens array exhibited remarkable polarization-dependent optical properties. Generally, this work may open new avenues toward the fabrication of micropatterned single crystals for various optical applications and shed light on fundamental mechanisms in biomineralization.

Supporting Information

Supporting Information is available from the Wiley Online Library or from the author.

Acknowledgements

This work was supported by NSFC (Grant Nos. 21173010, 21473004, and 51121091) and MOST (Grant No. 2013CB932601).

[1] H. A. Lowenstam, S. Weiner, *On Biomineralization*, Oxford University Press, New York, **1989**.
[2] F. Nudelman, N. A. Sommerdijk, *Angew. Chem. Int. Ed.* **2012**, *51*, 6582.
[3] J. Aizenberg, A. Tkachenko, S. Weiner, L. Addadi, G. Hendler, *Nature* **2001**, *412*, 819.
[4] F. C. Meldrum, H. Cölfen, *Chem. Rev.* **2008**, *108*, 4332.
[5] a) Y.-Y. Kim, K. Ganesan, P. Yang, A. N. Kulak, S. Borukhin, S. Pechook, L. Ribeiro, R. Kröger, S. J. Eichhorn, S. P. Armes, B. Pokroy, F. C. Meldrum, *Nat. Mater.* **2011**, *10*, 890; b) Y. Liu, W. Yuan, Y. Shi, X. Chen, Y. Wang, H. Chen, H. Li, *Angew. Chem. Int. Ed.* **2014**, *53*, 4127.
[6] a) F. Natalio, T. P. Corrales, M. Panthöfer, D. Schollmeyer, I. Lieberwirth, W. E. Müller, M. Kappl, H.-J. Butt, W. Tremel, *Science* **2013**, *339*, 1298; b) D. Gebauer, *Angew. Chem. Int. Ed.* **2013**, *52*, 8208.
[7] J. Aizenberg, D. A. Muller, J. L. Grazul, D. Hamann, *Science* **2003**, *299*, 1205.
[8] a) R. J. Park, F. C. Meldrum, *Adv. Mater.* **2002**, *14*, 1167; b) B. Wucher, W. Yue, A. N. Kulak, F. C. Meldrum, *Chem. Mater.* **2007**, *19*, 1111; c) N. B. J. Hetherington, A. N. Kulak, K. Sheard, F. C. Meldrum, *Langmuir* **2006**, *22*, 1955; d) N. B. J. Hetherington, A. N. Kulak, Y.-Y. Kim, E. H. Noel, D. Snoswell, M. Butler, F. C. Meldrum, *Adv. Funct. Mater.* **2011**, *21*, 948; e) A. S. Finnemore, M. R. J. Scherer, R. Langford, S. Mahajan, S. Ludwigs, F. C. Meldrum, U. Steiner, *Adv. Mater.* **2009**, *21*, 3928; f) C. Lu, L. Qi, H. Cong, X. Wang, J. Yang, L. Yang, D. Zhang, J. Ma, W. Cao, *Chem. Mater.* **2005**, *17*, 5218; g) C. Li, L. Qi, *Angew. Chem. Int. Ed.* **2008**, *47*, 2388; h) C. Li, L. Qi, *Adv. Mater.* **2010**, *22*, 1494.
[9] S. Yang, G. Chen, M. Megens, C. K. Ullal, Y. J. Han, R. Rapaport, E. L. Thomas, J. Aizenberg, *Adv. Mater.* **2005**, *17*, 435.
[10] a) K. Lee, W. Wagermaier, A. Masic, K. P. Kommareddy, M. Bennet, I. Manjubala, S. W. Lee, S. B. Park, H. Colfen, P. Fratzl, *Nat. Commun.* **2012**, *3*, 725; b) I. Schmidt, K. Lee, E. Zolotoyabko, P. Werner, T. S. Shim, Y.-K. Oh, P. Fratzl, W. Wagermaier, *ACS Nano* **2014**,*8*, 9233.
[11] M. Cho, M. Daneshpanah, I. Moon, B. Javidi, *Proc. IEEE* **2011**, *99*, 556.
[12] L. Zhang, Y. Yang, X. Zhao, Z. Fang, X. Yuan, *Opt. Express* **2012**, *20*, 26021.
[13] R. Bitterli, T. Scharf, H.-P. Herzig, W. Noell, N. de Rooij, A. Bich, S. Roth, K. J. Weible, R. Voelkel, M. Zimmermann, *Opt. Express* **2010**, *18*, 14251.
[14] D. Schmid, T.-Y. Huang, S. Hazrat, R. Dirks, O. Hosten, S. Quint, D. Thian, P. G. Kwiat, *Opt. Express* **2013**, *21*, 15538.
[15] P. Nussbaum, R. Voelkel, H. P. Herzig, M. Eisner, S. Haselbeck, *Pure. Appl. Optics* **1997**, *6*, 617.
[16] Y. Sun, S. R. Forrest, *Nat. Photon.* **2008**, *2*, 483.
[17] Y.-K. Ee, P. Kumnorkaew, R. A. Arif, H. Tong, J. F. Gilchrist, N. Tansu, *Opt. Express* **2009**, *17*, 13747.
[18] J. J. Schwartz, S. Stavrakis, S. R. Quake, *Nat. Nanotechnol.* **2010**, *5*, 127.
[19] Y. M. Song, Y. Xie, V. Malyarchuk, J. Xiao, I. Jung, K.-J. Choi, Z. Liu, H. Park, C. Lu, R.-H. Kim, *Nature* **2013**, *497*, 95.
[20] X. Li, Y. Ding, J. Shao, H. Tian, H. Liu, *Adv. Mater.* **2012**, *24*, OP165.
[21] J. Yong, F. Chen, Q. Yang, G. Du, H. Bian, D. Zhang, J. Si, F. Yun, X. Hou, *ACS Appl. Mater. Interfaces* **2013**, *5*, 9382.
[22] Y. L. Sun, W. F. Dong, R. Z. Yang, X. Meng, L. Zhang, Q. D. Chen, H. B. Sun, *Angew. Chem. Int. Ed.* **2012**, *124*, 1590.
[23] a) M. Yaegashi, M. Kinoshita, A. Shishido, T. Ikeda, *Adv. Mater.* **2007**, *19*, 801; b) Y. H. Kim, J. O. Lee, H. S. Jeong, J. H. Kim, E. K. Yoon, D. K. Yoon, J. B. Yoon, H. T. Jung, *Adv. Mater.* **2010**, *22*, 2416.
[24] M. Erdélyi, M. Bereznai, G. Gajdátsy, Z. Bor, *Opt. Commun.* **2008**, *281*, 4807.
[25] J. Z. Salvail, M. Agnew, A. S. Johnson, E. Bolduc, J. Leach, R. W. Boyd, *Nat. Photon.* **2013**, *7*, 316.
[26] J. Aizenberg, G. Hendler, *J. Mater. Chem.* **2004**, *14*, 2066.
[27] X. Ye, L. Qi, *Nano Today* **2011**, *6*, 608.

[28] C. Li, G. Hong, P. Wang, D. Yu, L. Qi, *Chem. Mater.* **2009**, *21*, 891.
[29] Y. Luo, L. Sonnenberg, H. Cölfen, *Cryst. Growth Des.* **2008**, *8*, 2049.
[30] A. B. D. Nandiyanto, A. Suhendi, O. Arutanti, T. Ogi, K. Okuyama, *Langmuir* **2013**, *29*, 6262.
[31] J. Yeom, K. Hong, S.-g. Park, J. Hong, S.-W. Min, B. Lee, *Opt. Express* **2013**, *21*, 31189.

Received: September 13, 2014
Revised: September 30, 2014
Published online: November 3, 2014